Nonstationary Motor Fault Detection Using Recent Quadratic Time–Frequency Representations

Satish Rajagopalan, *Member, IEEE*, José A. Restrepo, *Member, IEEE*, José M. Aller, Thomas G. Habetler, *Fellow, IEEE*, and Ronald G. Harley, *Fellow, IEEE*

***Abstract*—As the use of electric motors increases in the aerospace and transportation industries where operating conditions continuously change with time, fault detection in electric motors has been gaining importance. Motor diagnostics in a nonstationary environment is difficult and often needs sophisticated signal processing techniques. In recent times, a plethora of new time–frequency distributions has appeared, which are inherently suited to the analysis of nonstationary signals while offering superior frequency resolution characteristics. The Zhao–Atlas–Marks distribution is one such distribution. This paper proposes the use of these new time–frequency distributions to enhance nonstationary fault diagnostics in electric motors. One common myth has been that the quadratic time–frequency distributions are not suitable for commercial implementation. This paper also addresses this issue in detail. Optimal discrete-time implementations of some of these quadratic time–frequency distributions are explained. These time–frequency representations have been implemented on a digital signal processing platform to demonstrate that the proposed methods can be implemented commercially.**

***Index Terms*—Choi–Williams distribution (CWD), condition monitoring, eccentricity, fault diagnosis, motors, rotor faults, time–frequency analysis, Zhao–Atlas–Marks (ZAM).**

I. Introduction

FAULT detection in electric motors operating under nonstationary operating conditions has been gaining importance in recent times due to the fact that motors used in most applications, such as actuators in the aerospace and transportation industries, operate under conditions that rapidly vary with time. Such applications demand increased reliability from electric motors, and motor condition monitoring can help improve reliability by providing early warning of an impending fault condition. Electric motors operating under continuously changing speed and load conditions have voltages and currents whose frequency and amplitude are constantly changing. Diagnostics of motor faults under such conditions is a challenging problem due to the need for the application of sophisticated signal processing techniques that can process nonstationary signals. Nonstationary signal analysis techniques have been applied to track fault signatures in the stator current of motors operating in such transient conditions where the motor's speed and load are continuously changing with time [1], [2]. The short-time Fourier transform (STFT), which is a linear time–frequency representation (TFR), is one such technique that has been widely used due to its robustness and simplicity [1], [2]. The STFT is however dependent on the type and length of the window as it has to be chosen as a tradeoff between time and frequency resolution.

Quadratic TFRs have been recently proposed as an alternative to STFT due to their independence from the choice or size of the window and their inherent suitability to nonstationary signals. The Wigner–Ville distribution (WVD) and its variants, particularly the smoothed pseudo-WVD (SPWVD), have been suggested as possible choices [3], [4]. However, these distributions come with their own drawbacks. They generate interference terms called cross terms in addition to the original frequency components (also called autoterms). These nonnegligible cross-term artifacts in the time–frequency spectrum can interfere with the actual fault frequencies, thereby diminishing the ability to precisely determine the severity of the fault. Modifications to the WVD, namely, the SPWVD, attempt to suppress the cross terms but at the cost of frequency resolution.

However, in recent times, there has been a plethora of new time–frequency distributions that provide strong cross-term suppression while offering superior frequency resolution characteristics. The Choi–Williams distribution (CWD) and the Zhao–Atlas–Marks (ZAM) distribution are examples [5], [6]. There have also been new techniques to improve the readability of traditional quadratic time–frequency distributions such as the reassigned SPWVD. While [2]–[4] investigated the use of time–frequency distributions in rotor fault detection under continuously changing motor operating conditions, the focus of this paper is to improve nonstationary fault diagnostics in electric motors by exploring the use of these newer and more recently developed time–frequency distributions. One common myth has been that the quadratic time–frequency distributions are not suitable for commercial implementation. This paper also addresses this issue in detail. Optimal discrete-time implementations of some of these quadratic time–frequency distributions are explained. These TFRs have been implemented on a digital signal processing (DSP) platform to demonstrate that the proposed methods can be implemented

Paper IPCSD-07-081, presented at the 2006 Industry Applications Society Annual Meeting, Tampa, FL, October 8–12, and approved for publication in the IEEE Transactions on Industry Applications by the Electric Machines Committee of the IEEE Industry Applications Society. Manuscript submitted for review February 17, 2007 and released for publication October 17, 2007. This work was supported by Duke Power Company, Charlotte, NC.

S. Rajagopalan, T. G. Habetler, and R. G. Harley are with the School of Electrical and Computer Engineering, Georgia Institute of Technology, Atlanta, GA 30332 USA (e-mail: satish.r@ieee.org; thabetler@ee.gatech.edu; ron.harley@ece.gatech.edu).

J. A. Restrepo is with the Departamento de Electrónica y Circuitos, Universidad Simón Bolívar, Caracas 1080-A, Venezuela (e-mail: restrepo@usb.ve).

J. M. Aller is with the Departamento de Conversión y Transporte de Energía, Universidad Simón Bolívar, Caracas 1080-A, Venezuela (e-mail: jaller@usb.ve).

Digital Object Identifier 10.1109/TIA.2008.921431

TABLE I
SOME WELL-KNOWN TFRS AND THEIR KERNELS

TFR	Kernel: $\varphi(\xi,\tau)$
WVD	1
PWVD (Windowed or Pseudo WVD)	$h(\tau)$
Spectrogram	$\int h\left(u+\frac{\tau}{2}\right)h^*\left(u-\frac{\tau}{2}\right)e^{j2\pi\xi u}du$

commercially. These algorithms are developed for automotive applications where the use of a fast digital signal processor is possible. The fault detection algorithms can also be integrated into industrial adjustable-speed drives where sophisticated digital signal processors/microprocessors are already present for motion control. The processing times of these algorithms are not excessively large due to the fast processors available today. Moreover, in most motor diagnostics applications, latency is typically not a concern as motor condition monitoring is performed over long intervals of time, which are usually every 30 min or 1 h.

II. QUADRATIC TFRS FOR NONSTATIONARY BLDC MOTOR FAULT DIAGNOSTICS

Time–frequency analysis is the 3-D time, frequency, and amplitude representation of a signal, which is inherently suited to indicate transient events in a signal. In 1966, Cohen developed a generalized form of phase-space distribution from which all other time–frequency distributions could be derived. These distributions are essentially energy distributions as they distribute the energy of the signal over the two description variables: time and frequency. As the energy is a quadratic function of the signal, the Cohen class time–frequency energy distributions are quadratic representations. These distributions can be used for the analysis of true nonstationary signals without any underlying assumptions. The general form of the Cohen's class of distributions [or also called as the generalized time–frequency distributions (GTFD)] for a signal $f(t)$ is given by [7]

$$D(t,\omega;\varphi)=\iiint e^{j(\xi\mu-\tau\omega-\xi t)}\varphi(\xi,\tau)\times f\left(\mu+\frac{\tau}{2}\right)f^*\left(\mu-\frac{\tau}{2}\right)d\mu d\tau d\xi \quad (1)$$

where $\varphi(\xi,\tau)$ is a kernel that defines the time–frequency transformation, t is the instantaneous time, and ω is the instantaneous frequency. τ, ξ, and μ are the running time, frequency, and position variables used in the integration, respectively. Table I depicts some well-known TFRs and their respective kernels, where $h(\tau)$ is a time window (Gaussian, Hamming, etc.).

The choice of a time kernel appropriate to a specific application can be better explained through the generalized ambiguity function (GAF). Equation (1) can be rewritten in terms of the GAF [8], i.e., GAF$(\xi,t:\varphi)$, as follows:

$$D(t,\omega,\varphi)=\frac{1}{4\pi^2}\iint \mathrm{GAF}(t,\omega:\varphi)e^{-j(\xi t+\tau\omega)}d\xi d\tau \quad (2)$$

where the GAF is described by

$$\mathrm{GAF}(\xi,t:\varphi)=\varphi(\xi,\tau)\int_{-\infty}^{\infty} f\left(\mu+\frac{\tau}{2}\right)f^*\left(\mu-\frac{\tau}{2}\right)e^{-j\xi\mu}d\mu = \frac{\varphi(\xi,\tau)}{2\pi}\int_{-\infty}^{\infty} F\left(\nu+\frac{\xi}{2}\right)F^*\left(\nu-\frac{\xi}{2}\right)e^{j\nu\tau}d\nu. \quad (3)$$

In (2), the GTFD $D(t,\omega,\varphi)$ is the double Fourier transform of GAF$(\xi,t:\varphi)$. Thus, it can be seen that the GAF is the dual of the GTFD in the sense of the Fourier transform. The property of interest is the one relating to the interference geometry. For a multicomponent signal, the elements of the GAF corresponding to autoterms are mainly located around the origin, whereas the interference components or cross terms are located away from the origin, at a distance that is proportional to the time–frequency distance between the autoterms.

Therefore, considering the continuously changing time–frequency structure of the current signal in an electric machine, the best suited time–frequency distribution is the one that selects a region around the origin in the ambiguity domain and reduces to zero away from the origin. The distributions, which are also known as reduced interference distributions, depend on the product of ξ and τ to provide this kind of selection. Examples of these distributions are the CWD, the Born–Jordan (BJ) distribution, and the ZAM or cone-shaped distribution. The kernel functions for these distributions have been recreated in the ambiguity domain through simulation and appear in Fig. 1(a)–(c). This figure shows the spread of the kernels over the cross terms and autoterms. The autoterms are near the origin; however, the cross terms that are usually present away from the origin are diminished by the kernels. The spread of the ZAM kernel in Fig. 1(c) suppresses the cross terms more effectively than the BJD and CWD kernels.

As mentioned before, the spectral content of the motor stator current is changing, and although the reduced interference distributions produce good results, a better approach would be to use an adaptive optimal kernel [9]. The procedure is based on the adaptation of a radial Gaussian kernel over a short-time ambiguity function around the time instant of interest [9]. This procedure is computationally more demanding since it requires an additional adaptation step that fixed kernel distributions do not have. In any case, the use of an adaptive kernel provides information over the relative quality of the results provided by the fixed kernel distributions.

III. RECENT TIME–FREQUENCY KERNELS

Several reduced interference distributions have since been proposed, which are all a subset of the Cohen's class. Some

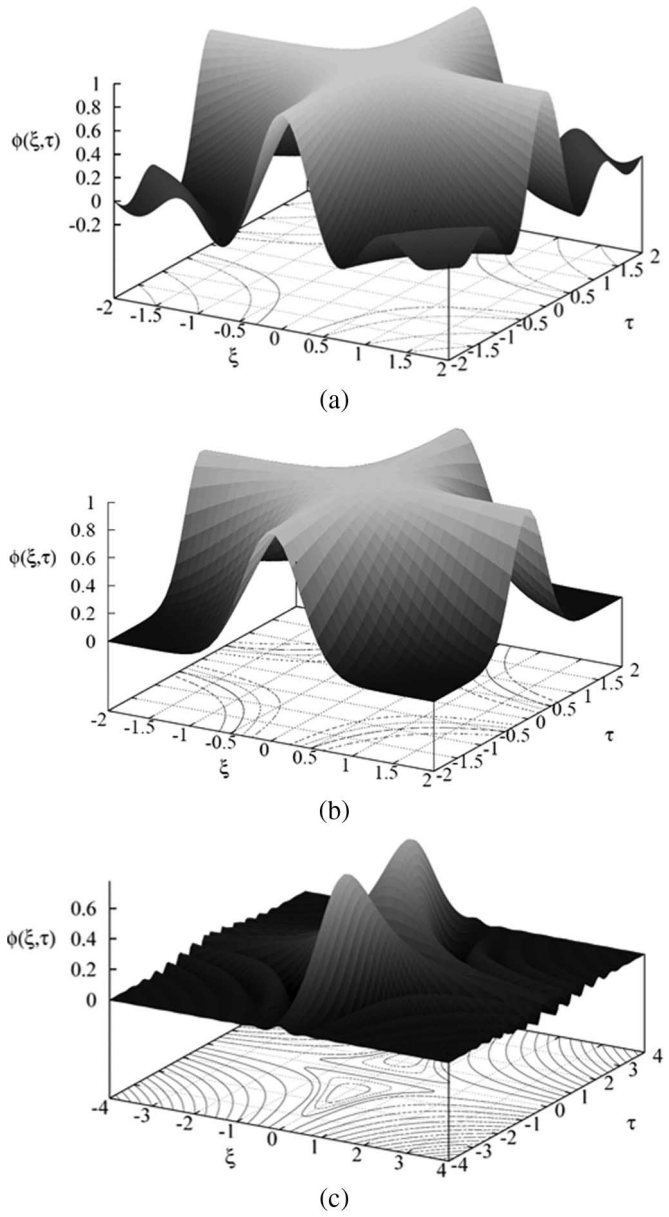

Fig. 1. Kernel function in the ambiguity domain for (a) the CWD, (b) the BJ distribution, and (c) the ZAM distribution.

of these distributions are Margenau–Hill, Kirkwood–Rihaczek, BJ, ZAM, and CWD [10].

The exponential kernel function or the Choi–William kernel has the same dimensions as the ambiguity function. The exponential kernel function suppresses the cross terms away from the horizontal and vertical axes. Therefore, the CWD reduces the cross terms generated by two autoterms with different time and frequency centers. The CWD has a coarser time–frequency resolution than the WVD because the CWD also blurs the autoterms whereas the WVD just reduces the cross terms. The Choi–William exponential kernel is given as

$$\varphi(\xi,\tau) = e^{-\xi^2\tau^2/\sigma} \tag{4}$$

where the parameter σ determines the tradeoff between the cross-term suppression and the frequency resolution. If σ has a large value, then the kernel is effectively one and results in the WVD. A smaller σ, on the other hand, enhances the actual frequency components in the signal (also termed as autoterms) while suppressing the cross terms.

The ZAM distribution is a relatively new distribution [6]. While the emphasis on development of distributions such as the CWD was to meet marginal conditions and other properties [10], the development of the ZAM "cone kernel" was intended to introduce finite time support and reduce cross terms [10]. The kernel to be used in (1) to obtain a ZAM distribution is

$$\varphi(\xi,\tau) = \varphi_1(\tau)\frac{\sin\left(\xi|\tau|/a\right)}{\xi/2} \tag{5}$$

where $\varphi_1(\tau)$ is a function to be specified (usually taken to be equal to one), and a is greater than or equal to two. The cone-shaped kernel function suppresses the cross terms away from the vertical axis and the origin of the ambiguity function plane. The BJ distribution is similar to the ZAM distribution. The ZAM distribution is nothing but a BJ distribution (6) with finite time support and is smoothed along the frequency axis

$$\varphi(\xi,\tau) = \frac{\sin(\xi\tau)}{\xi\tau/2}. \tag{6}$$

IV. BLDC Motor Fault Diagnostics Using Quadratic TFRs

Quadratic time–frequency distributions explained in the previous section are now applied to extract nonstationary fault frequency signatures from the electric motor (a brushless DC motor (BLDCM) is used in this paper as an example) current by using the well-known "motor current signature analysis" technique [11]. This technique is based on the fact that rotor faults, such as dynamic eccentricity or unbalanced rotors, produce unique characteristic fault frequency signatures in the motor current spectra. For example, in BLDCMs operating at constant speed, the dynamic eccentricity fault frequencies present in the stator current are given by [12]

$$f_{\rm rf} = f_e \pm k\frac{f_e}{P/2} \tag{7}$$

where $f_{\rm rf}$ is the rotor fault frequency, f_e is the fundamental frequency, P is the number of poles in the BLDC machine, and k is any integer. These fault frequencies are also present when the current is in a nonstationary state and are tracked by using the proposed quadratic TFR-based detection algorithm shown in Fig. 2. The BLDC stator current is square wave in nature and contains higher order power harmonics $(6n+1,\ n=1,2,3\ldots)$. Unwanted cross terms that may mask motor fault frequencies may be created due to the interaction of these harmonic frequencies. Hence, the acquired BLDC stator current is first filtered adaptively by using an adaptive tracking filter to remove the fundamental frequency and other inverter harmonics. This selective adaptive filtering prevents cross terms from being introduced at frequencies of interest. The TFR spectrum of a real-valued signal has both positive and negative frequency components, and this produces cross

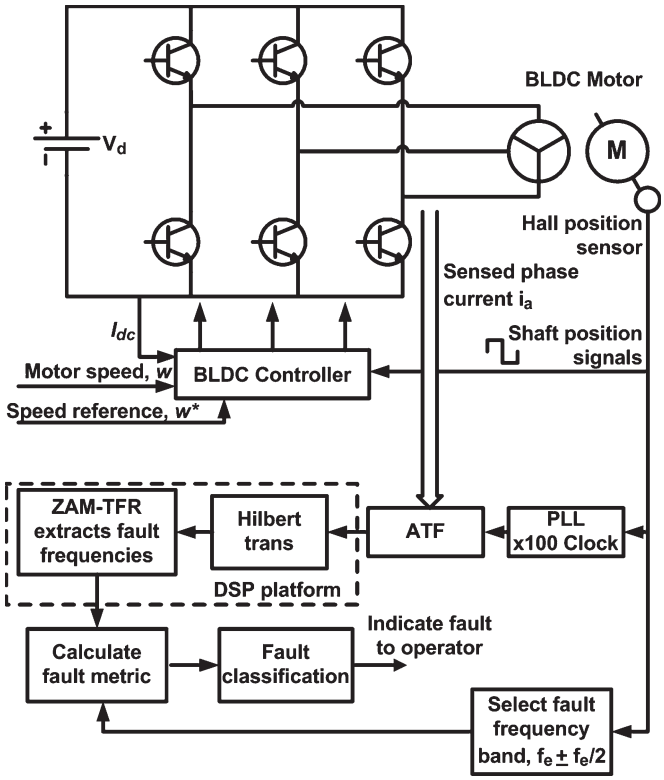

Fig. 2. Fault detection in BLDCMs using TFRs.

terms between those negative and positive frequencies. The stator current, being a real-valued signal, suffers from this problem. These cross terms can be eliminated by eliminating the negative frequency terms. This is achieved by converting the real-valued current signal into an analytic signal using a Hilbert transformation [2], [3], [13]. The fault frequencies are then extracted from this analytic signal by computing the ZAM distribution (one and five). If needed, other TFRs such as the CWD can be used instead of the ZAM distribution.

A simple fault metric is then calculated by computing the root-mean-square (rms) value of the instantaneous amplitudes of the extracted fault frequencies for a preselected band. Several individual bands with their respective rms metrics can be computed to separate multiple fault frequencies. This metric is used to indicate a developing rotor fault. Thresholds can be set to determine the severity of the fault and provide an indication to the operator to take some necessary precautionary action. The faults investigated in this paper are dynamic eccentricity and unbalanced rotors, although the proposed technique can be extended to other faults such as bearing defects, broken rotor bars in induction motors, and load defects.

V. Evaluation of Selected Time–Frequency Kernels

To illustrate the performance of the aforementioned signal processing techniques, a test signal i_a approximating a stator current of a motor with a rotor fault is used. By assuming that the fault is dynamic eccentricity, the fault frequencies in a six-pole motor occur at two-thirds and four-thirds of the fundamental frequency $p(t)$. The test signal in (8) represents the stator

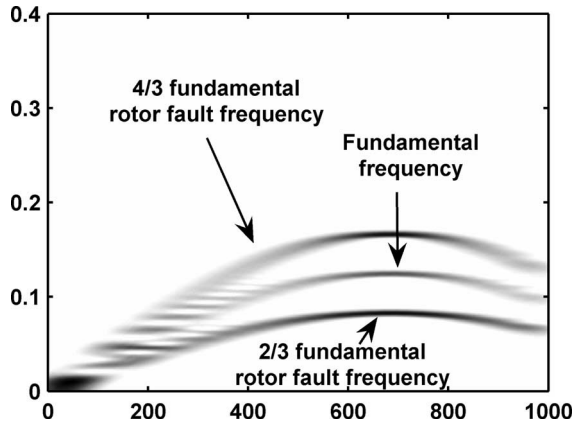

Fig. 3. STFT of simulated BLDCM rotor fault comprising of three frequencies varying over time.

current of a six-pole motor with dynamic eccentricity and is modeled as a sum of three frequency components comprising of the fundamental frequency $p(t)$ and the two fault frequencies at two-thirds and four-thirds of $p(t)$. The fundamental frequency has an amplitude of 0.05 amp (corresponding to a filtered stator current) with the two rotor fault frequency components, each having an amplitude of 0.07 amp. The amplitudes in (8) are chosen arbitrarily to imitate a rotor fault scenario as closely as possible

$$i_a = 0.05\cos\left(2\pi p(t)t\right) + 0.07\cos\left(4\pi p(t)t/3\right) + 0.07\cos\left(8\pi p(t)t/3\right). \quad (8)$$

A 1-s record with 2048 samples of this i_a waveform is used for comparing the various signal processing techniques. The frequency $p(t)$ is varied sinusoidally between 0 and 120 Hz as in (9), as would typically occur in a BLDC nonstationary servo motor application

$$p(t) = \sin(2\pi ft), \quad \text{where } f = 120 \text{ Hz}. \quad (9)$$

The Rice University Time–Frequency (t–f) Analysis toolbox [13] for MATLAB is used to compute the Wigner distributions for the simulated motor current signal. This toolbox has specific functions tailor-made for time–frequency analysis. Fig. 3 shows a spectrogram (STFT) of the signal i_a, and it shows the varying values in kilohertz of the three frequencies of (8) along the Y-axis, as a function of time along the X-axis, for the 1-s data. Darker zones in the spectrogram represent higher amplitudes. The window $h(\tau)$ of the spectrogram in Table I is chosen as a Hamming window with a length of 0.25 s. The frequency resolution of the spectrogram is poor in the low-frequency region as the three frequencies of (8) cannot be distinguished from each other when the fundamental frequency drops below 60 Hz. It can also be seen from Fig. 3 that the spectral components produced by the STFT are smeared (or thick) in the frequency domain. Hence, the fault frequencies are not sharply localized but spread over a frequency range.

Fig. 4 shows the PWVD of the same test signal i_a. The frequencies are concentrated in a thin band indicating an excellent concentration of energy, but the presence of strong cross terms may produce false fault alarms. The CWD in Fig. 5

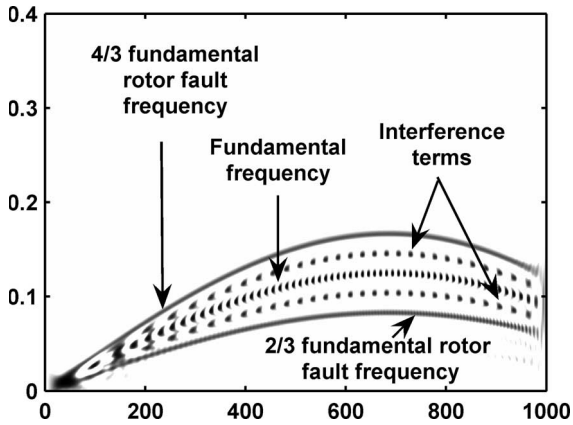

Fig. 4. PWVD of simulated BLDCM rotor fault comprising of three frequencies varying over time.

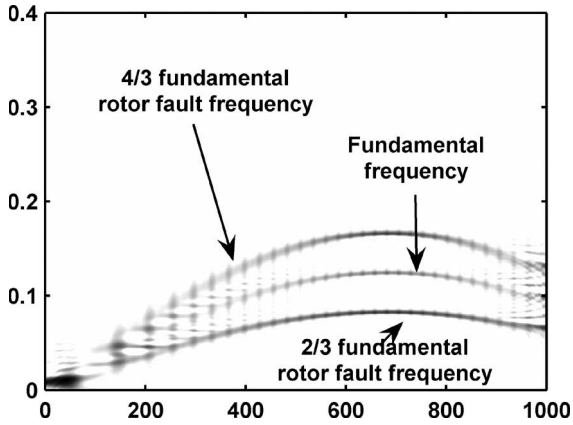

Fig. 5. CWD of simulated BLDCM rotor fault comprising of three frequencies varying over time.

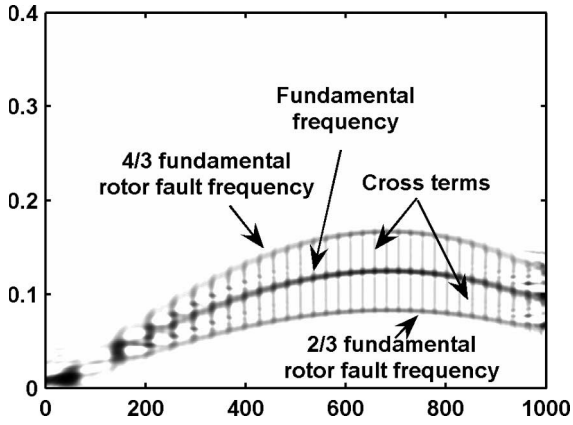

Fig. 6. BJD of simulated BLDCM rotor fault comprising of three frequencies varying over time.

$(\sigma = 1)$ has better energy concentration than the STFT, but the frequency resolution in the low-frequency region (below 50 Hz) is compromised to obtain good cross-term suppression.

The BJ distribution of the same test signal, which is calculated by using the Rice University t–f toolbox, is shown in Fig. 6. Even though the frequency resolution is very good (all three frequencies are distinctly tracked), the distribution still suffers from cross terms. The ZAM distribution in Fig. 7,

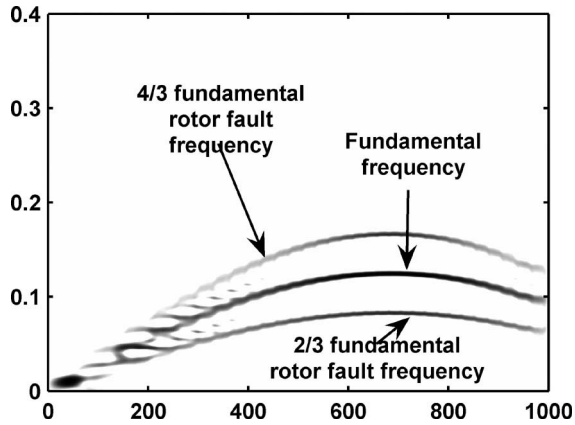

Fig. 7. ZAM of simulated BLDCM rotor fault comprising of three frequencies varying over time.

on the other hand, shows good energy concentration (low-frequency smear), excellent cross-term suppression, and much better frequency resolution than the spectrogram of Fig. 3.

VI. BLDCM Fault Diagnostics Using Quadratic TFRs—Experimental Results

Experimental results are also obtained to demonstrate the viability of using the CWD and ZAM distributions as tools for nonstationary motor fault detection. A six-pole 12-V 1-kW BLDCM with speed and current control is used in the experiments. One of the phase currents is sensed by using a Hall current sensor. A high attenuation (56 dB) switch-capacitor analog filter is used to adaptively filter out the fundamental frequency and all harmonics that are larger than twice the fundamental frequency, from the BLDC stator current prior to the data acquisition. The filter is composed of a sixth-order elliptic notch filter that attenuates the fundamental component and an eighth-order Butterworth filter that removes all harmonics above two. Clocking for the filter is obtained from the BLDCM's Hall position sensors using a phase-locked loop that tracks the fundamental frequency of current. The analog filter was preferred over the digital filter due to the ease of implementation, as analog chip-level filter solutions are readily available from many semiconductor manufacturers. The construction of the filter is explained in detail in [2].

The hardware setup for the nonstationary motor operation test, including the implementation of the dynamic eccentricity and the unbalanced rotor, is explained in detail in [2]. The speed reference of the BLDCM is varied sinusoidally or in a triangular pattern of 0–15 Hz to obtain a nonstationary motor operation. This frequency range adequately represents the nonstationarity encountered in several practical applications, including those encountered in transportation industries. The speed varies cyclically from 600 to 1800 r/min. The acquired data were sampled at 2 kHz, and the signals are analyzed by using data slices of length 4096 samples (approximately 2 s).

For a six-pole BLDCM, the main rotor fault frequencies for both the dynamic eccentricity and the unbalanced rotor occur at two-thirds and four-thirds times the fundamental frequency [$k = 1$ in (7)]. Smaller harmonics at one-third and five-thirds

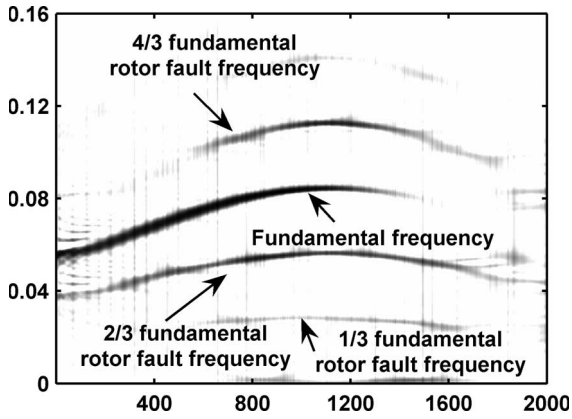

Fig. 8. CWD of filtered BLDCM (with mechanical unbalanced rotor) stator current and 3-Hz sine speed reference.

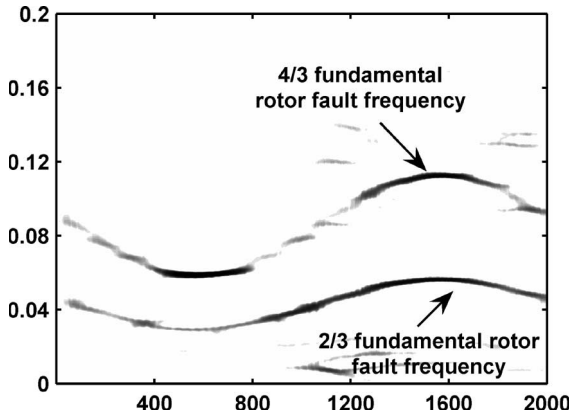

Fig. 9. ZAM of filtered BLDCM (with dynamic eccentricity) stator current and 5-Hz sinusoidal speed reference.

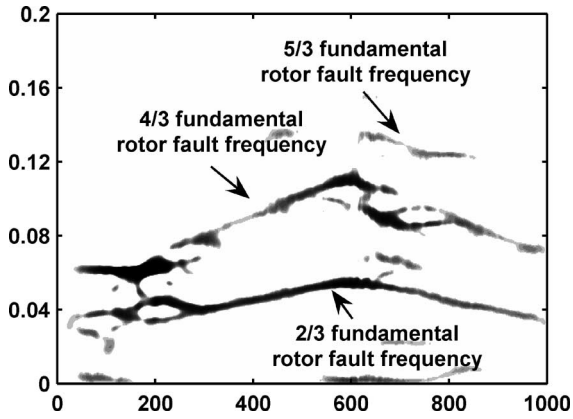

Fig. 10. ZAM of filtered BLDCM (with dynamic eccentricity) stator current and 10-Hz triangular speed reference.

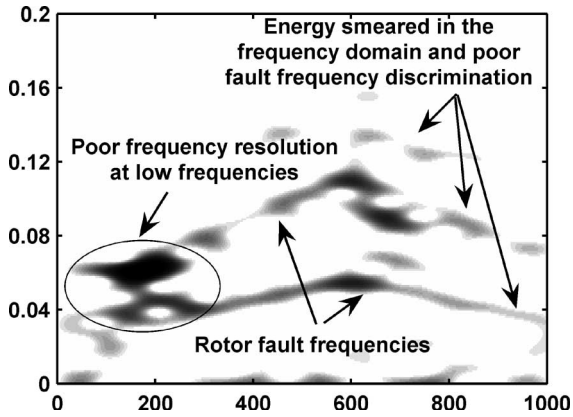

Fig. 11. STFT of filtered BLDCM (with dynamic eccentricity) stator current and 10-Hz triangular speed reference.

the fundamental frequency [$k = 2$ in (7)] may also exist. The Rice University t–f toolbox [14] is again used to calculate the TFRs of the filtered BLDC current signal. Fig. 8 shows the CWD of the filtered stator current of an unbalanced BLDCM operating with a 3-Hz sinusoidal speed reference. The rotor unbalance was created by using an unbalanced disk mounted on the motor shaft [2]. Some small fundamental frequency components still exist because the adaptive filter used for this experiment only had a limited attenuation (36 dB). The fault frequencies are distinctly tracked in time.

Fig. 9 shows the ZAM distribution of the filtered stator current of a dynamically eccentric BLDCM (32% dynamic air-gap eccentricity) now operating with a 5-Hz sinusoidal speed reference. The high attenuation (56 dB) adaptive notch filter is used here, and hence, no fundamental component can be seen in Fig. 9. Again, the ZAM distribution tracks the fault frequencies distinctly over time. The ZAM distribution's good frequency resolution, sharp energy concentration, and ability to handle nonstationary signals are important advantages in fast-changing nonstationary signals. To demonstrate these advantages, the ZAM distribution of the filtered stator current signal of the same dynamically eccentric BLDCM (Fig. 10), operating with a 10-Hz triangular speed reference, is compared with the STFT of the same signal (Fig. 11). This STFT is computed by using a Hamming window with a size of 0.25 s. This length is obtained through trial and error so as to obtain a good compromise between the time and frequency resolutions for this problem and the obtained experimental data. The ZAM distribution distinctly tracks the fault frequencies in the filtered stator current. The ZAM energy concentration in Fig. 10 is sharp, and the frequency resolution at low frequencies is better than in Fig. 11 for the STFT.

Similarly, the performance of the ZAM is studied at a more stringent nonstationary condition. Fig. 12 shows the ZAM distribution for the filtered stator current of a dynamically eccentric BLDCM operating with a 15-Hz sinusoidal speed reference. The fault frequencies are again distinctly tracked over time. The frequency resolution and the energy concentration of the algorithm are better than those of the STFT. The ZAM again distinguishes itself in its ability to resolve highly nonstationary signals. Fig. 13 shows that as the nonstationarity increases, the STFT suffers from more and more frequency and time resolution problems even with carefully chosen window types and length.

Fig. 14 shows a simple rms fault metric calculated for both a good BLDCM and a faulty BLDCM with dynamic eccentricity. This rms fault metric is obtained by calculating the instantaneous rms value of the fault frequency amplitudes

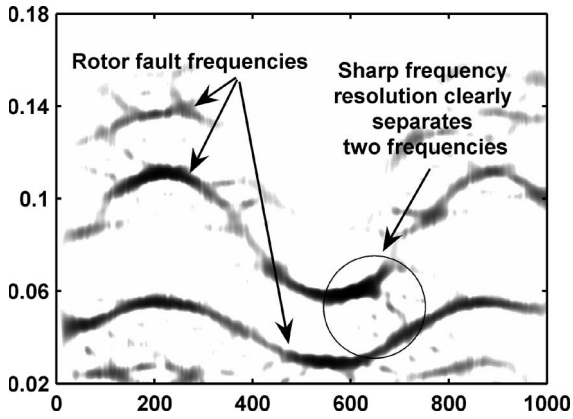

Fig. 12. ZAM of filtered BLDCM (with dynamic eccentricity) stator current and 15-Hz sinusoidal speed reference.

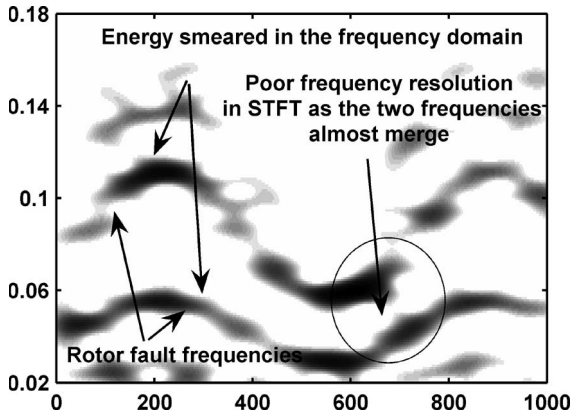

Fig. 13. STFT of filtered BLDCM (with dynamic eccentricity) stator current and 15-Hz sinusoidal speed reference.

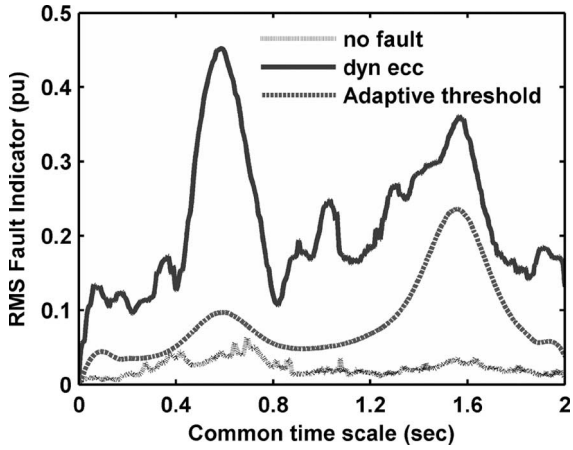

Fig. 14. RMS fault indicator discriminates the BLDC rotor eccentricity using an adaptive threshold (5-Hz sinusoidal speed reference).

extracted by using the ZAM distribution from the filtered BLDCM stator current. In both of these cases (Fig. 14), the BLDCM is operating with a 5-Hz sinusoidal speed reference. An adaptive threshold that varies as a fixed percentage of the fundamental frequency component (in this case, it is chosen as 2%) is used for the automatic detection of rotor faults. The rms fault metric of the defective BLDCM is significantly different than the rms fault metric of a good motor. Fig. 14 also shows that the adaptive threshold effectively discriminates the fault over time when compared with a good motor.

VII. Commercial Implementation of Quadratic TFRs for BLDCM Fault Diagnostics

One common mistaken belief has been that the recent quadratic TFRs are not suitable for commercial implementation due to their complexity. The TFRs are implemented on an ADSP21369-SHARC DSP operating with a 331.776-MHz core clock, and the time taken for computing one time slice of information is recorded by using an oscilloscope.

For a practical implementation of distribution members of Cohen's class, the generalized discrete-time discrete frequency distribution (GDTDFD) is defined as [15]

$$\hat{D}(l,\theta;\hat{\Phi}) = \sum_{n=-\infty}^{+\infty} R_l(n)e^{-j2n\theta} \tag{10}$$

where $\hat{D}(l,\theta;\hat{\Phi})$ is the GDTDFD, l and θ are the discrete equivalents of time and frequency, respectively, and $\hat{\Phi}$ is the discrete kernel that defines the type of time–frequency distribution. $R_l(n)$ is an autocorrelation of the data sequence s and is given as

$$R_l(n) = \sum_{m=-\infty}^{+\infty} s(l+m+n)s^*(l+m-n)\hat{\Phi}(m,2n) \tag{11}$$

where m and n are similar to running time and frequency variables. In practice, only a finite span in time of the signal is available. Therefore, the aforementioned equations can be practically realized by applying a sliding window to the signal under analysis. Equations (10) and (11) can be rewritten as

$$\tilde{D}(l,\theta;\hat{\Phi}) = \sum_{n=-N}^{+N} R_l(n)e^{-j2n\theta} \tag{12}$$

and

$$R_l(n) = \sum_{m=-M}^{+M} s_a(l+m+n)s_a^*(l+m-n)\hat{\Phi}(m,2n). \tag{13}$$

In (13), $s_a(n)$ represents the analytic version of the original signal $s(n)$. The analytic signal $s_a(n)$ has only positive frequency components in the frequency spectrum, and thereby, the use of this signal reduces any artifacts that may be created due to the interaction of the positive and negative frequency components that are present in the spectrum of the original real-valued signal. The analytic signal is defined as

$$s_a(n) = s(n) + j\mathrm{H}\{s(n)\} \tag{14}$$

where $\mathrm{H}\{s(n)\}$ is the Hilbert transform of the signal $s(n)$.

The autocorrelation $R_l(n)$ is first computed by using (13) for a finite data sequence and kernel of lengths N and M,

TABLE II
COMPUTATION TIME FOR QUADRATIC TFR KERNELS ($N = M = 64$)

TFR	Computation time for processing data slice of length 129 (in μ-sec)
Spectrogram	10
GDTDFD (CW, BJ and ZAM)	220
ZAM (Optimized)	98

respectively. The length N is chosen based on the desired frequency resolution, and the length M is selected based on the shape of the kernel in the ambiguity domain and is dependent on the available memory and computational speed of the data processor (usually a digital signal processor). The time–frequency spectrum of the signal is then computed from the discrete Fourier transform (DFT) of $R_l(n)$. The DFT can be efficiently computed by using standard fast Fourier transform (FFT) algorithms. The computation is further optimized by evaluating two successive $R_l(n)$ sequences $R_{l1}(n)$ and $R_{l2}(n)$ together [16] as

$$R_{l\text{comb}} = R_{l1}(n) + jR_{l2}(n). \tag{15}$$

The DFT of the individual sequences can be evaluated by using a single DFT for the combined autocorrelation shown in (15), thus halving the number of final FFTs used.

A. Implementation of ZAM, BJ, and CW Distributions

The time taken for the computation of the reduced interference distribution for one time slice of data is measured on an oscilloscope and is compared in Table II for $N = M = 64$ points. The Hilbert filter for computing the analytic signal is implemented by using an 81-tap finite-impulse response filter. The ZAM distribution is compared with the BJ, the CWD, and the STFT. The amount of computation in the ZAM algorithm, for a 64-point FFT and a 64-point correlation window, is as follows. The correlation matrix update requires $(2^*N = 128)$ additions and $(4^*N = 256)$ products. The computation of the correlation vector requires $(2^*N^2 = 8192)$ additions and $(2^*N^2 = 8192)$ products. The computationally intensive part of the algorithm, apart from the FFT, is the correlation computation.

The actual algorithm implementation uses the same operations for different kernels as specified by the discrete set of equations, namely, (10)–(15). The computational time, which is required by the DSP to compute the time–frequency spectrum of one data sequence (of length 129 in this case) using this set of discrete equations that define the GDTDFD and various time–frequency kernels, is shown in Table II. The computational time required for processing the same data sequence using the spectrogram (STFT) is also shown in Table II. The practical implementation was carried out on an ADSP21369 with a 331.776-MHz core-clock DSP board. The computational times for all the kernels are similar.

The algorithm can be further optimized for individual kernels. For example, the ZAM kernel is optimized by using a circular matrix to compute the correlation matrix. The intricate details of this implementation are beyond the scope of this paper, but suffice it to say that the optimization makes use of the symmetry in the distributions to reduce the computations by half. The computational time measured for this optimization is also shown in Table II. It is important to note that the results in Table II are specifically for the data lengths specified ($N = M = 64$). Changing the data length or the FFT length would change the computational time.

The algorithm uses the following data arrays in computing a time–frequency slice:

1) four N-point arrays for the FFT;
2) four N-point arrays for a complex signal $R_l(n)$;
3) two $(2N + 1)$ arrays for the analytic signal $s_a(n)$;
4) two $(N + 1) * (M + 1)$ matrices for holding a temporal correlation information for computing (13).

The size of the data arrays remains the same for both the generalized and the optimized implementations. Therefore, the memory consumed also remains the same.

B. Critical Comparison of TFR-, Frequency-Domain-, and Time-Domain-Based Methods

Most time-domain modeling techniques can effectively model stationary stochastic models but cannot model nonstationary phenomena. In these cases, the signal may be separated into small windows, and the previously mentioned time-domain techniques may be employed. However, accurate modeling is difficult due to the difficulties in modeling and the choice of model order. Due to these complexities, frequency/time–frequency-based methods are considered as better options due to their ability to directly extract the fault frequencies of interest. While frequency-domain-based methods such as the Fourier transform cannot be directly used on nonstationary signals, simple adaptations such as the STFTs can be used. Table II shows that the processing time of the STFT (a linear time–frequency distribution) is smaller than that of the quadratic TFRs. The STFTs also consume lesser memory than quadratic TFRs. However, as shown in Figs. 10 and 11, the frequency discrimination of the STFTs is poorer than the quadratic TFRs. Therefore, in applications where nonstationary behavior is severe and processing power is not constrained, the quadratic TFRs are a better choice.

VIII. REASSIGNED TIME–FREQUENCY DISTRIBUTIONS

Another method of further improving the performance of TFRs is the use of reassignment. In a reassigned SPWV, the computed values of a regular SPWV are moved to an alternate time–frequency plane depending on the instantaneous frequency and time delay [17]. The reassignment method automatically compresses the energy in the quadratic TFR toward the

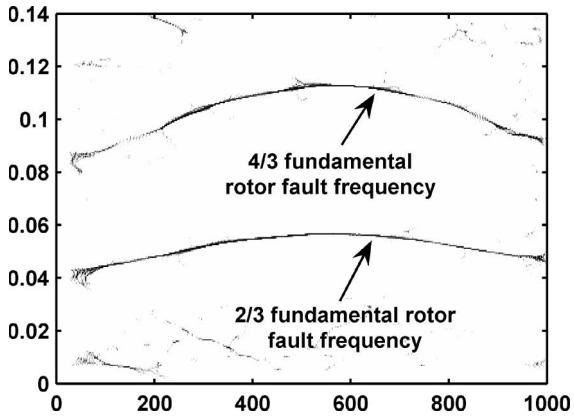

Fig. 15. Reassigned SPWV of filtered BLDCM (with dynamic eccentricity) stator current and 5-Hz sinusoidal speed reference.

centers of gravity of the signal components to make the signal components more concentrated. Fig. 15 shows the reassigned SPWV of a part of the motor stator current signal shown in Fig. 9 and shows much better frequency concentration than a regular TFR.

IX. Conclusion

This paper has presented the use of new advances in nonstationary signal analysis, particularly quadratic time–frequency distributions, toward rotor fault detection in BLDCMs. Recent distributions, such as the ZAM distribution, offer superior performance when compared with traditional techniques such as the STFT. This was demonstrated through both simulation and experimental results. The reason behind the good performance of these distributions is that they are designed with an emphasis on improving frequency/time resolution and cross-term suppression rather than on satisfying the marginal properties of a traditional t–f distribution. The quadratic TFRs provide much better frequency resolution and localization of energy with the ZAM distribution exhibiting the best performance. In particular, the CWD is a good tradeoff between the excellent frequency resolution of the WVD and the high cross-term suppression of the ZAM distribution. One of the most important advantages of the quadratic distribution is that these distributions do not depend on any parameter similar to the size or type of the window as is the case for the spectrogram (STFT).

The detection of dynamic eccentricity and unbalanced rotor in BLDCMs is specifically illustrated in this paper as an example. However, the proposed method can be extended to detect other faults such as bearing faults, gear faults, and broken rotor bars in induction motors.

A common belief is that these new distributions are too complicated to be implemented in a commercial system due to their perceived intense computational time. To address this issue, the time–frequency distributions have been implemented on a DSP platform. While the computational time for these distributions is greater than for the conventional techniques such as the STFT, this is not of a significant concern as motor faults develop slowly and motor condition monitoring is performed over long intervals of time. As a result, any condition monitoring technique is usually not a burden on the computational/memory capability of the DSP. Hence, the computational times presented in this paper for quadratic TFR algorithms should not be a burden when integrated into a commercial system. Therefore, it would be prudent to choose the method that would provide the highest frequency and time resolution. The computational time can be further decreased by paralleling several microprogrammed systems and using more optimized software algorithms as has been demonstrated in this paper.

Acknowledgment

The authors wish to acknowledge the support of Delphi Corporation, Troy, MI, and in particular the help of Dr. T. Sebastian (Delphi Saginaw Steering Systems) and Dr. B. Lequesne and Dr. T. W. Nehl (Delphi Research Labs).

References

[1] B. Yazici and G. B. Kliman, "An adaptive statistical time–frequency method for detection of broken bars and bearing faults in motors using stator current," *IEEE Trans. Ind. Appl.*, vol. 35, no. 2, pp. 442–452, Mar./Apr. 1999.

[2] S. Rajagopalan, J. M. Aller, J. A. Restrepo, T. G. Habetler, and R. G. Harley, "Diagnosis of rotor faults in brushless DC (BLDC) motors operating under non-stationary conditions using windowed Fourier ridges," in *Conf. Rec. 40th IEEE IAS Annu. Meeting*, Hong Kong, 2005, pp. 26–33.

[3] S. Rajagopalan, J. A. Restrepo, J. M. Aller, T. G. Habetler, and R. G. Harley, "Wigner–Ville distributions for detection of rotor faults in brushless DC (BLDC) motors operating under non-stationary conditions," in *Proc. Int. SDEMPED*, Vienna, Austria, 2005. CD-ROM.

[4] M. Blodt, M. Chabert, J. Regnier, and J. Faucher, "Mechanical load fault detection in induction motors by stator current time–frequency analysis," *IEEE Trans. Ind. Appl.*, vol. 42, no. 6, pp. 1454–1463, Nov./Dec. 2006.

[5] H. I. Choi and W. J. Williams, "Improved time–frequency representation of multi-component signals using exponential kernels," *IEEE Trans. Acoust., Speech, Signal Process.*, vol. 37, no. 6, pp. 862–871, Jun. 1989.

[6] Y. Zhao, L. E. Atlas, and R. J. Marks, II, "The use of cone-shaped kernels for generalized time–frequency representations of nonstationary signals," *IEEE Trans. Acoust., Speech, Signal Process.*, vol. 38, no. 7, pp. 1084–1091, Jul. 1990.

[7] L. Cohen, "Generalized phase-space distribution functions," *J. Math. Phys.*, vol. 7, no. 5, pp. 781–786, May 1966.

[8] L. Cohen and T. E. Posch, "Generalized ambiguity functions," in *Proc. IEEE ICASSP*, 1985, pp. 1033–1036.

[9] D. L. Jones and R. G. Baraniuk, "An adaptive optimal-kernel time–frequency representation," *IEEE Trans. Signal Process.*, vol. 43, no. 10, pp. 2361–2371, Oct. 1995.

[10] F. Hlawatsch and G. F. Boudreaux-Bartels, "Linear and quadratic time–frequency signal representations," *IEEE Signal Process. Mag.*, vol. 9, no. 2, pp. 21–67, Apr. 1992.

[11] G. B. Kliman and J. Stein, "Methods of motor current signature analysis," *Electr. Mach. Power Syst.*, vol. 20, no. 5, pp. 463–474, Sep. 1992.

[12] S. Rajagopalan, W. le Roux, R. G. Harley, and T. G. Habetler, "Diagnosis of potential rotor faults in brushless DC machines," in *Proc. 2nd Int. Conf. PEMD*, Edinburgh, U.K., 2004, pp. 668–673.

[13] B. Boashash, *Time–Frequency Signal Analysis—Methods and Applications*. Melbourne, Australia: Longman Cheshire, 1992, p. 26.

[14] F. Auger, P. Flandrin, P. Goncalvès, O. Lemoine, *Time–Frequency Toolbox for Use With MATLAB Reference Guide.* CNRS France/Rice University, 1996. [Online]. Available: http://tftb.nongnu.org/refguide.pdf

[15] J. Restrepo, T. A. de Perez, M. I. G. de Guzmán, and V. M. Guzmán, "DSP implementation of an AC-machine sensorless speed measurement system using the Wigner distribution," in *Proc. 7th EPE*, Trondheim, Norway, 1997, pp. 4.524–4.528.

[16] B. Boashash and P. J. Black, "An efficient real-time implementation of the Wigner–Ville distribution," *IEEE Trans. Acoust., Speech, Signal Process.*, vol. ASSP-35, no. 11, pp. 1611–1618, Nov. 1987.

[17] F. Auger and P. Flandrin, "Improving the readability of time–frequency and time-scale representations by the reassignment method," *IEEE Trans. Signal Process.*, vol. 43, no. 5, pp. 1068–1089, May 1995.

Satish Rajagopalan (S'99–M'01) received the B.E. degree in electrical engineering from the University of Madras, Chennai, India, in 1997, the M.S. degree in electrical engineering from Iowa State University, Ames, in 2000, and the Ph.D. degree from the Georgia Institute of Technology, Atlanta, in 2006.

His research interests are in switching power converter technology, motor control, and motor condition monitoring.

Dr. Rajagopalan is a member of the IEEE Industry Applications, IEEE Power Electronics, and IEEE Industrial Electronics Societies.

José A. Restrepo (S'89–M'92) received the B.Sc. and M.Sc. degrees in electronics engineering from the Universidad Simón Bolívar, Caracas, Venezuela, in 1988 and 1991, respectively, and the Ph.D. degree from the University of Manchester Institute of Science and Technology, Manchester, U.K., in 1996.

He is currently a Full Professor of electronics engineering with the Departamento de Electrónica y Circuitos, Universidad Simón Bolívar. His research interests include advanced control of electrical machines, artificial intelligence, and digital signal processors applied to motion control.

José M. Aller was born in Caracas, Venezuela, in 1958. He received the Ing. degree in electrical engineering from the Universidad Simón Bolívar, Caracas, in 1980, the M.S. degree in electrical engineering from the Universidad Central de Venezuela, Caracas, in 1982, and the Ph.D. degree in industrial engineering from the Universidad Politécnica de Madrid, Madrid, Spain, in 1993.

He has been a Lecturer with the Universidad Simón Bolívar for 26 years, where he is currently a Full-Time Professor with the Departamento de Conversión y Transporte de Energía. He was the General Secretary of the Universidad Simón Bolívar between 2001 and 2005. His research interests include space vector application, electrical machine control, and power electronics.

Thomas G. Habetler (S'85–M'89–SM'92–F'02) received the B.S. and M.S. degrees in electrical engineering from Marquette University, Milwaukee, WI, in 1981 and 1984, respectively, and the Ph.D. degree from the University of Wisconsin, Madison, in 1989.

From 1983 to 1985, he was a Project Engineer with the Electro-Motive Division, General Motors. Since 1989, he has been with the School of Electrical and Computer Engineering, Georgia Institute of Technology, Atlanta, where he is currently a Professor of electrical engineering. He is a regular consultant to industry in the field of condition-based diagnostics for electrical systems. His research interests include electric machine protection and condition monitoring, switching converter technology, and drives. He has published over 150 papers in the field.

Dr. Habetler currently serves as the IEEE Division II Director-Elect, is the Past-President of the IEEE Power Electronics Society, and is the Past-Chair of the Industrial Power Converter Committee of the IEEE Industry Applications Society. He was the recipient of four conference prize paper awards from the IEEE Industry Applications Society.

Ronald G. Harley (M'77–SM'86–F'92) received the M.Sc.Eng. degree in electrical engineering (*cum laude*) from the University of Pretoria, Pretoria, South Africa, in 1965, and the Ph.D. degree from London University, London, U.K., in 1969.

In 1971, he was appointed to the Chair of Electrical Machines and Power Systems, University of Natal, Durban, South Africa, and later, he became the Department Head and the Deputy Dean of Engineering. He is currently the Duke Power Company Distinguished Professor with the School of Electrical and Computer Engineering, Georgia Institute of Technology, Atlanta. He has coauthored some 400 papers and three patents. His research interests include the dynamic behavior and condition monitoring of electric machines, motor drives, power systems and their components, and controlling them by the use of power electronics and intelligent control algorithms.

Dr. Harley is a Fellow of the British Institution of Electrical Engineers. He is also a Fellow of the Royal Society in South Africa and a Founder Member of the Academy of Science in South Africa formed in 1994. During 2000 and 2001, he was one of the IEEE Industry Applications Society's six Distinguished Lecturers. He was the Vice-President of Operations of the IEEE Power Electronics Society from 2003 to 2004 and the Chair of the Atlanta Chapter of the IEEE Power Engineering Society. He is currently the Publications Chair for the IEEE Power Electronics Society and the Chair of the Distinguished Lecturers and Regional Speakers program of the IEEE Industry Applications Society. He was the recipient of the Cyrill Veinott Award in 2005 from the IEEE Power Engineering Society for his "outstanding contributions to the field of electromechanical energy conversion." Ten of his coauthored papers have also attracted prizes from journals and conferences.